Ma, Xiaopeng; Phi Van, Valerie; Kimm, Melanie A.; Prakash, Jaya; Kessler, Horst; Kosanke, Katja; Feuchtinger, Annette; Aichler, Michaela; Gupta, Aayush; Rummeny, Ernst J.; Eisenblätter, Michel; Siveke, Jens; Walch, Axel K.; Braren, Rickmer; Ntziachristos, Vasilis; Wildgruber, Moritz:

Integrin-Targeted Hybrid Fluorescence Molecular Tomography/X-ray Computed Tomography for Imaging Tumor Progression and Early Response in Non-Small Cell Lung Cancer

DOI: http://dx.doi.org/10.1016/j.neo.2016.11.009

URN: urn:nbn:de:hbz:464-20170823-111532-4

Link: https://duepublico.uni-duisburg-essen.de:443/servlets/DocumentServlet?id=44365

Source: Neoplasia, 2017, 19(1), pp. 8-16; available online 7 December 2016.

NEOPLASIA
www.neoplasia.com

Volume 19 Number 1 January 2017 pp. 8–16 8

Integrin-Targeted Hybrid Fluorescence Molecular Tomography/X-ray Computed Tomography for Imaging Tumor Progression and Early Response in Non-Small Cell Lung Cancer[1]

Xiaopeng Ma[*,2], Valerie Phi Van[†,2], Melanie A. Kimm[†], Jaya Prakash[*], Horst Kessler[‡], Katja Kosanke[†], Annette Feuchtinger[§], Michaela Aichler[§], Aayush Gupta[¶], Ernst J. Rummeny[†], Michel Eisenblätter[#], Jens Siveke[¶,,††], Axel K. Walch[§], Rickmer Braren[†], Vasilis Ntziachristos[*] and Moritz Wildgruber[†,#]**

*Institute for Biological and Medical Imaging, Helmholtz Zentrum München, Ingolstädter Landstrasse 1, D-85764 Oberschleissheim, Germany; [†]Department of Radiology, Klinikum Rechts der Isar, Technische Universität München, Ismaningerstrasse 22, D-81675, München, Germany; [‡]Chemistry Department and TUM Institute for Advanced Study, Lichtenbergstrasse 2a, D-85748, Garching, Germany; [§]Research Unit Analytical Pathology, Helmholtz Zentrum München, Ingolstädter Landstrasse 1, D-85764 Oberschleissheim, Germany; [¶]Department of Internal Medicine II, Klinikum Rechts der Isar, Technische Universität München, Ismaningerstrasse 22, D-81675, München, Germany; [#]Department of Clinical Radiology, Universitätsklinikum Münster, Albert-Schweitzer-Campus 1, D-48149, Münster, Germany; **German Cancer Consortium (DKTK) and German Cancer Research Center (DKFZ), Im Neuenheimer Feld 280, D-69120, Heidelberg, Germany; [††]Division of Solid Tumor Translational Oncology, German Cancer Consortium (DKTK), partner site Essen, University Hospital Essen, Hufelandstraße 55, D-45147 Essen, Germany

Abstract

Integrins play an important role in tumor progression, invasion and metastasis. Therefore we aimed to evaluate a preclinical imaging approach applying αvβ3 integrin targeted hybrid Fluorescence Molecular Tomography/X-ray Computed Tomography (FMT-XCT) for monitoring tumor progression as well as early therapy response in a syngeneic murine Non-Small Cell Lung Cancer (NSCLC) model. Lewis Lung Carcinomas were grown orthotopically in C57BL/6 J mice and imaged in-vivo using a αvβ3 targeted near-infrared fluorescence (NIRF) probe. αvβ3-targeted FMT-XCT was able to track tumor progression. Cilengitide was able to substantially block the binding of the NIRF probe and suppress the imaging signal. Additionally mice were treated with an established chemotherapy regimen of Cisplatin and Bevacizumab or with a novel MEK inhibitor (Refametinib) for 2 weeks. While μCT revealed only a moderate slowdown of tumor growth, αvβ3 dependent signal decreased significantly compared to non-treated mice already at one week post treatment. αvβ3 targeted imaging might therefore become a promising tool for assessment of early therapy response in the future.

Neoplasia (2017) 19, 8–16

Address all correspondence to: Moritz Wildgruber MD, PhD, Translational Research Imaging Center, Institut für Klinische Radiologie, Universitätsklinikum Münster, Albert-Schweitzer-Campus 1, Gebäude A16.
E-mail: moritz.wildgruber@ukmuenster.de

[1] Funding: The work was supported by the Deutsche Forschungsgemeinschaft (SFB 824).
[2] These authors contributed equally to this study.

Received 13 October 2016; Revised 14 November 2016; Accepted 14 November 2016

1476-5586
http://dx.doi.org/10.1016/j.neo.2016.11.009

Introduction

Despite advances in therapy, lung cancer remains the leading cause of cancer mortality worldwide [1]. The most common type of lung cancer is Non-Small Cell Lung Cancer (NSCLC), which compromises a variety of subtypes such as adenocarcinomas, squamous cell and large cell carcinomas. The prognosis of NSCLC is dependent on primary tumor growth, as well as tumor invasion and metastasis [2]. Three major steps have to be passed for tumor invasion and metastasis to occur: first, tumor cells need to detach from their cellular surrounding and invade into the interstitial stroma. Subsequently, cancer cells have to penetrate the vessel wall and intravasate into the circulation, either into the blood or the lymphatic system. Lastly, metastatic cells have to extravasate into the target tissue followed by progressive proliferation at the seeding site [3]. For each of these processes, integrins play a central role and therefore have been identified as key mediators of cancer invasion and metastasis. Integrins, consisting each of two type I transmembrane subunits (α and β) transmit both mechanical and chemical signals. Besides reorganization of the cytoskeleton during cell adhesion and migration, integrin signaling is additionally important for controlling cell survival and proliferation [3]. Another prerequisite for tumor growth and spread is neoangiogenesis [4]. Besides allowing the tumor to grow beyond a limited size, angiogenesis similarly constitutes a gateway for tumor cell intravasation and extravasation of tumor-associated leukocytes [3]. Also for tumor angiogenesis integrins have been shown to play a decisive role [5]. Integrins can be highly up regulated in tumor cells, angiogenic and activated endothelial cells as well as on tumor associated macrophages. The latter have been shown to elicit a central role in promoting neovascularisation by sensing hypoxia in avascular areas of the tumor and reacting by a consecutive boost in production and secretion of angiogenic growth factors such as vascular endothelial growth factor (VEGF) [6]. Various integrins such as αvβ3, α5β1 and αvβ6 have been evaluated as prognostic biomarkers for lung cancer progression [2,7]. Adding anti-angiogenic agents targeting integrin mediated neoangiogenesis to conventional chemotherapy regimens has shown beneficial effect in progression free survival [8], Similarly, drugs targeting integrins themselves show first promising effects when added to established chemotherapy approaches. Cilengitide, a RGD (arginine, glycine, aspartic acid) based competitive inhibitor of αvβ3 and αvβ5 integrins has been shown a trend for increased progression free survival in NSCLC patients [9]. These first encouraging results warrant further investigation into the use of specific inhibition of integrins and their subsequent downstream effects in pursuit of a successful therapy for NSCLC. Development of such targeted therapies requires specific tools to evaluate and monitor specific effects of individualized cancer therapies. Targeted imaging in molecular and cellular oncology allows precise assessment of cancer biomarkers, showing their activity dynamically in vivo and over time [10]. Targeted imaging of αvβ3 expression has been evaluated using various technologies applying RGD based nuclear tracers [11,12], nanoparticles [13,14] and optical fluorescence probes [15]. Activated αvβ3 was successfully visualized by positron emission tomography (PET) in cancer patients by ^{18}F–galacto-RGD [16]. We have previously demonstrated that αvβ3 targeted fluorescence imaging allows early detection of neoplastic lesions in a transgenic K-ras mouse model of NSCLC with high sensitivity [15]. In the present study we demonstrate that αvβ3 targeted molecular imaging is able to detect αvβ3 integrin expression similarly in a syngeneic orthotopic NSCLC mouse model using hybridized Fluorescence Molecular Tomography/X-ray Computed Tomography (FMT/–XCT) and that αvβ3 imaging is able to reveal biological responses to targeted therapy approaches. The first therapy regimen consisted of an established combination of Cisplatin and Bevacizumab, the second therapy approach was directed towards the Kras mutation, which is present in about 25% of NSCLC patients. Kras mutation predominantly results in the activation of the RAF–MEK-ERK pathway, which translates to a poor prognosis and a high risk of tumor resurgence. Here we use Refametinib (BAY 86–9766), a highly selective and potent orally available inhibitor of MEK 1 and MEK 2. We show an early imaging signature of biological tumor response to both therapy regimens before changes in tumor size occur.

Materials and Methods

Mice and Tumor Model

All animal experiments were approved by the local subcommittee on Research Animal Care (Protocol Number 49–10 and 69–14) and carried out in accordance with the Guide for the Care and Use of Laboratory Animals published by the U.S. National Institutes of Health (NIH publication No. 85–23, revised 1996). C57BL/6 J mice were purchased from Charles River Laboratories (Sulzbach, Germany). Lewis Lung Carcinoma cell line LLC1 (ATCC) were implanted intravenously by injecting 10^5 tumor cells (dissolved in 100 µl NaCl) intravenously into the tail vein. Tumor cells in this model start to grow to macroscopic visible tumor nodules at 3–5 weeks post injection. Imaging of mice was performed under full anesthesia using MMF (0,5 mg/kg Medetomidin, 5,0 mg/kg Midazolam, 0,05 mg/kg Fentanyl). Mice (n = 7) not receiving any treatment constituted the control group. These mice were imaged using a αvβ3 targeted fluorescence imaging probe (IntegriSense680, Perkin Elmer, Germany) with excitation/emission at peaks at 675 nm/693 nm, injected 24 h hours prior to imaging at a dose of 2 nmol/100 ml per 25 g mouse. For in vivo competition, respectively blocking experiments a group of mice (n = 5) was preinjected with 5 mg/kg cilengitide intravenously, 15 minutes before application of the fluorescence probe. In the chemotherapy group mice (n = 7) were treated for 2 weeks with a combination of cisplatin and bevacizumab (®Avastin), administered at 1.2 mg/kg daily and 5 mg/kg twice a week intraperitoneal, respectively. The second treatment group (n = 5) received Refametinib (BAY 86–9766) orally at 25 mg/kg daily for 5 days per week. Imaging in the chemotherapy groups was performed in the same manner as in the control group. After completion of imaging mice were euthanized with an overdose of Ketamin/Xylazine and the lungs were excised for further ex vivo analysis.

Study Protocol

After tumor implantation mice were scanned weekly by T2-weighted (T2w) MRI. MR imaging was performed on a 3T whole-body scanner (Ingenia, Philips Healthcare, Best, Netherlands) using an 8-channel wrist-coil. A 2D T2 weighted spin echo sequence was used with following parameters: FOV: 40 × 40 mm; matrix: 132 × 132; slice thickness: 0.7 mm; TE 101 ms; TR 2337 ms, flip angle 90°. After detection of a first macroscopically visible lesion, scanning was repeated every 2 days until the tumor size reached a diameter of 2 mm. When reaching the given tumor size, mice underwent hybrid FMT-XCT imaging at day 1, at day 5 to 7 and at day 11 to 14, after which the animals were sacrificed as described.

For competition experiments, mice received a first FMT-XCT imaging on day 3 after first macroscopic tumor growth after injection of αvβ3 targeted IntegriSense680. At day 5, mice were injected with the competitor/blocking agent cilengitide and 15 minutes later with IntegriSense680. Imaging was similarly performed at 24 h thereafter.

In the chemotherapy group, mice were imaged with FMT-XCT system on day 1 after the first macroscopic tumor growth was visible and chemotherapy was initiated immediately after completing the first FMT-XCT scan. Chemotherapy was continued as described above and mice received repeated FMT-XCT scans after injection with αvβ3 targeted IntegriSense680 at day 5 to 7 and 11 to 14. The study protocol is depicted in Figure. 1*A*, the course of tumor growth of the control group is shown in Figure 1*B*.

FMT-XCT Imaging

FMT-XCT data sets were collected by a previously built system presented [17]. The hybrid system was developed by incorporating a 360° free-space FMT system into a commercial micro-CT eXplore Locus XCT equipment (GE HealthCare, London, Canada), two systems are placed vertically on a full angle rotating gantry. The cone-beam XCT scanner system includes one X-ray illumination source and one X-ray detector. While the FMT component consists of three core parts: (1) Two diode laser sources (B&W Tek, Newark, USA) with the wavelength of 680 nm and 750 nm respectively, together with two optical fibers which were coupled to two separate optical collimators. The collimators focus the laser light to a spot as small as possible and shoot onto the specimen. (2) Before the transmitted laser light reaches into the CCD camera, one filter wheel is positioned before the camera. Different combination of long-pass filters and band-pass filters (Andover, Salem, NH) were fixed into the wheel to filter out the excitation light for fluorescence images or filter out the fluorescent wavelength light for excitation images. (3) All the excitation and emission (or fluorescence) images are captured and recorded by a back-illuminated cooled CCD camera (Princeton Instruments, Trenton, NJ), which coupled with a 50 mm lens (Carl Zeiss, Oberkochen, Germany). The sample mouse was placed on an epoxy bed, this specimen bed can hold tight the mouse, transfer it along the translation stage into the FMT-XCT system and position it precisely.

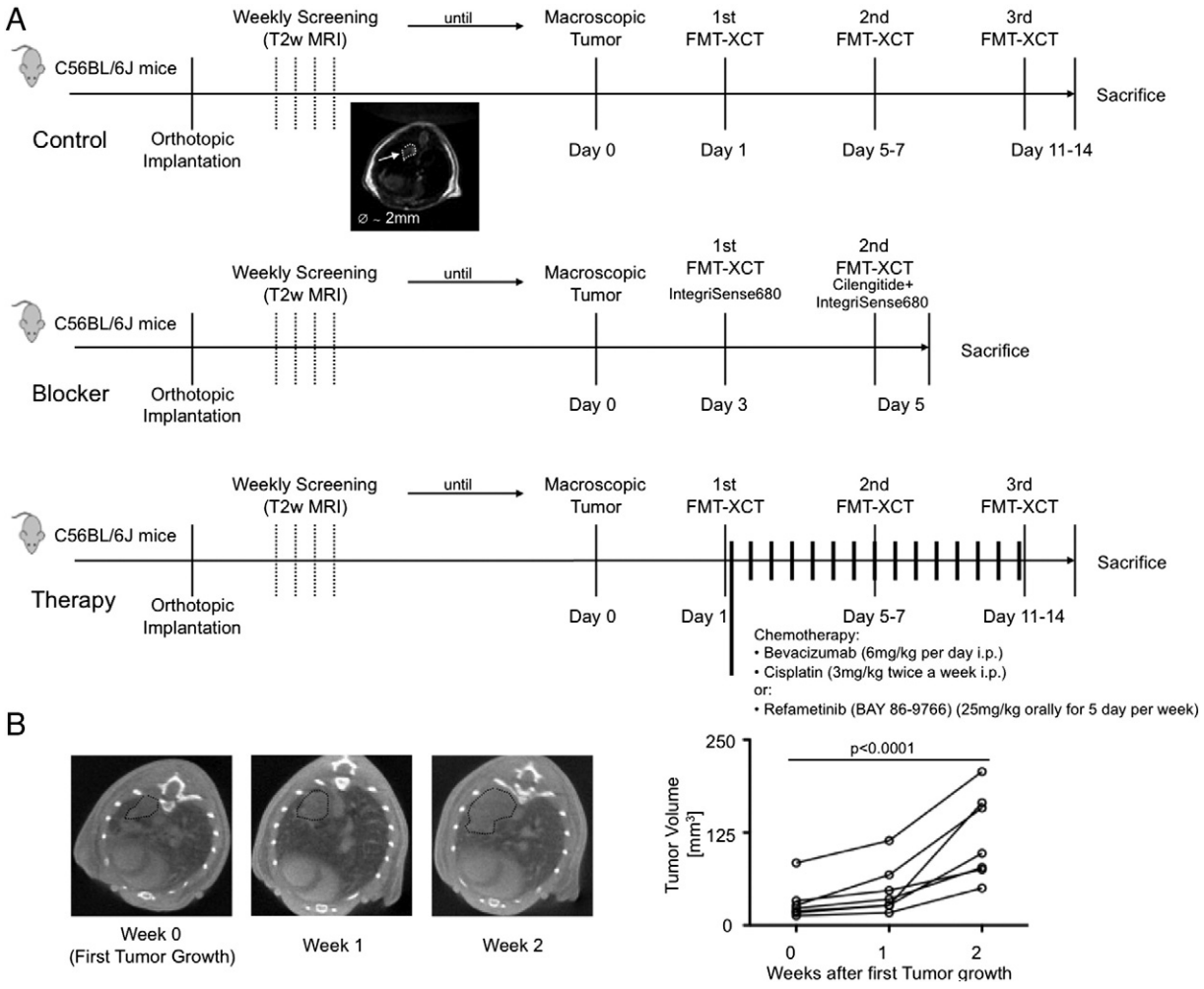

Figure 1. (A) Study design made up of three groups consisting of control mice, mice pre-treated with the RGD-based blocking agent (Cilengitide) and mice receiving either a combined chemotherapy treatment of Cisplatin and Bevacizumab or Refametinib monotherapy. After completion of imaging, mice were sacrificed and processed for further ex-vivo analysis (Histology/Immunohistochemistry, Flow Cytometry, Cryoslicing).(B) Course of orthotopic tumor growth on μCT imaging. When tumors reached the size of 2 mm in diameter, mice were subsequently investigated by hybrid FMT-XCT. Tumor volume increased almost exponentially with the mice having large tumor masses in both lungs at two weeks after initial tumor growth was observed.

The hybrid FMT-XCT dataset include two separate parts, FMT raw data and XCT raw data. FMT raw data were collected 360° with 18 locations of gantry (20° between each angle). For each gantry angle, three types of data were collected by CCD camera sequentially for analysis: one white front illumination image acquired by using a flat sheet white light in an epi-illumination mode. Then, for each angle, 20–50 laser source locations were calculated for the mouse and for each source location, excitation image and emission image were recorded by using 680 nm laser and corresponding filter sets. The laser power was set optimal automatically during the collection procedure. The whole scan time for FMT part was around 1 hour, which depended on mouse size, laser source location counts and fluorescence intensity inside of the specimen. The size of each FMT image, no matter white image, excitation image or fluorescence image, is high resolution with size 512 × 512 and SPE format (Princeton Instruments, Trenton, NJ, USA). XCT raw data, which is known as projections of the imaged sample, was collected after the FMT data acquisition. One typical XCT data set includes 400 projections for each specimen, with high resolution of 1750 × 914 and format of VFF file (Sun Microsystems, Inc., USA).

All FMT raw data and XCT projection raw data were stored and processed by self-programmed Matlab software. XCT projections were processed firstly for 3D reconstruction by a wrapped application from GE (evsbeam.exe) and Matlab programming. The generated 3D data VFF file was used for carrying out semi-automatic segmentation, the same was achieved by commercially available Amira software (Visage Imaging, Richmoud, Australia). Then, FMT-XCT inversion for solving sparse linear system of equations was performed using the least squares QR (LSQR) algorithm and normalized born ratios of excitation and emission images for all selected source-detector pairs. Amira was used to demonstrate the three dimensional location and size of underlying fluorescence source in the mouse body afterwards.

To compare the NIRF signal for αvβ3 in treated versus control mice the fluorescence ratio was normalized, with the initial value detected on day 1 before initiation of treatment was set to 100%.

Cryoslicing

A subgroup of sacrificed mice (n = 13) were frozen to −80 °C and embedded in a mixture of O.C.T. (Optimal Cutting Temperature) medium and India Ink. Cryoslice imaging of the mice was performed using a multispectral epi-illumination imaging system. For ~20 transversal slices per mouse, 250 μm apart, we acquired planar RGB images and planar fluorescence images using a filtered white light source and a sensitive CCD camera.

Immunohistochemistry and Fluorescence Microscopy

Lungs with implanted tumors were harvested and immediately shock frozen in liquid nitrogen. Serial sectioning for cryoslices was performed and mounted on glass slides. Sections were immunohistochemically stained for CD61 (BD Pharmingen; goat anti-hamster, Vector), CD51 (ENZO; goat anti-rabit, Vector) and CD31 (abcam; goat anti-rabit, Vector). Fluorescence was detected with an Axio Imager Z1 (Carl Zeiss, Jena, Germany) using Cy5.5 filter for the detection of IntegriSense and the DAPI filter for detection of nucleus staining by Hoechst 33,342.

Quantification of IntegriSense680 fluorescence was performed by image analysis using Definiens Developer XD2 software (Definiens AG; Munich, Germany). For each image the overall mean IntegriSense fluorescence intensity was calculated.

Flow Cytometry

To determine the cellular source of the IntegriSense680 signal, n = 3 mice were injected with the probe were sacrificed and the tumor-bearing lungs were processed for further analysis by flow cytometry, as previously described [18]. In brief, excised lungs were harvested, minced with fine scissors, and incubated in a cocktail of collagenase I, collagenase XI, DNase I, and hyaluronidase (Sigma-Aldrich) and digested at 37 °C for 1 h. Cells were then triturated through nylon mesh and centrifuged (15 min, 500*g*, 4°C). Single-cell suspensions were subsequently stained with propidium iodine and the following antibodies: FITC-CD61 (Clone C29. G2, BD Bioscience), APC-CD31 (Clone 13.3, BD Bioscience), Biotin-CD51 (RMV-7, BD Bioscience), the latter followed by secondary staining using PerCP-Streptavidin (BD Bioscience). Data were acquired on FACS Aria (BD Biosciences) with a 635 nm red laser and 685/LP and 695/40 BP filter configuration to detect IntegriSense680. FITC, APC and PerCP isotype controls were similarly obtained from BD Bioscience.

Statistics

Data are presented as mean ± SD. Group comparisons were performed by unpaired two-sided t-tests. Assessments of differences over time were determined by one-way ANOVA or in case of more than one group by two-way ANOVA, followed by Bonferroni post tests for multiple comparisons. $P < .05$ was considered significant.

Results

αvβ3 Expression in Lung Tumor Tissue

Lewis lung cell carcinomas were orthotopically grown in C57BL/6 J mice after intravenous injection. Tumors started to grow in both lungs, predominantly in the lower lobes to a macroscopic visible size at 3 to 5 weeks post implantation. When the first macroscopic solid tumor was detectable on MRI, tumors had a mean size of 30.9 ± 24.3 mm^3. Without therapy tumors exhibited a rapid growth albeit high standard deviation to 47.9 ± 33.6 mm^3 at 1 week and 118.6 ± 58.1 mm^3 at 2 weeks ($P < .0001$, one-way ANOVA, Figure 1*B*). To evaluate the potential of targeting αvβ3 in Lewis Lung Carcinoma we first confirmed integrin expression by solid tumors grown in vivo. Explanted tumors showed moderate expression of β3 (CD61) and strong expression of αv (CD51) (Figure 2*A*). Positive staining for αv and β3 was predominantly confined to the tumor cells themselves, with only moderate positivity for endothelial cells. Tumor-bearing mice were injected with the αvβ3 targeted fluorescent probe IntegriSense680. Positive near infrared fluorescence (NIRF) signal was predominantly emitted from the tumor cells, while normal lung tissue did not render a detectable NIRF signal. Detectable NIR fluorescence was significantly lower in mice pre-injected with a RGD blocking peptide (Cilengitide) before administration of the NIRF probe (n = 5, 34.6 ± 0.8 AU versus 44.9 ± 5.3 AU, $P = .046$ unpaired *t* test), similarly fluorescence was decreased in chemotherapy treated mice compared to controls (n = 7, 34.5 ± 5.8 AU versus 44.9 ± 5.3 AU, $P = .004$ unpaired *t* test, Figure 2*B*). Additionally we performed flow cytometry of cell suspensions obtained from digested tumors to further verify the cellular origin of the αvβ3 fluorescence signal (Figure 2*C*). Co-staining for CD31, CD51, (αv) and CD61 (β3) showed double positivity for αv and β3 in 22% of cells while tumor cells where positive for both integrin subunits in only 8%. Still tumor cells outnumbered endothelial cells (5.2 times more viable tumor than endothelial cells in cells suspensions). Flow cytometry

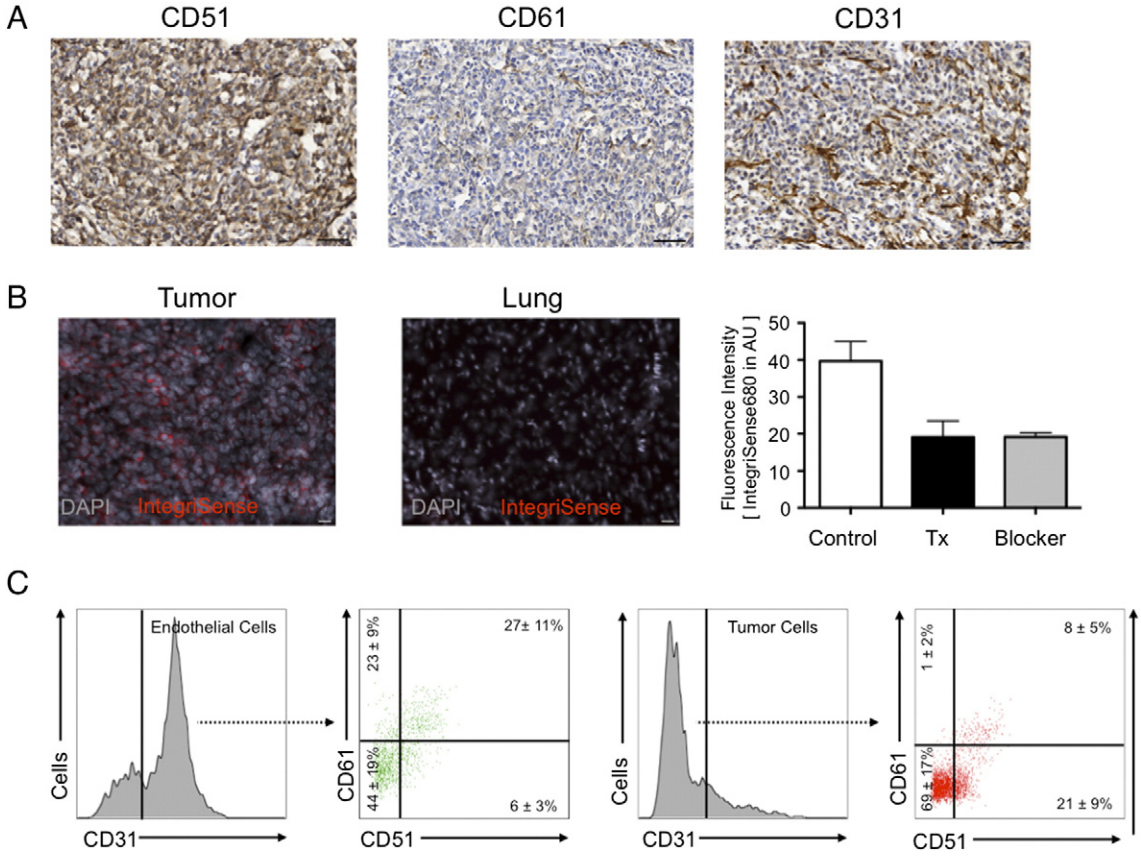

Figure 2. αvβ3 expression in orthotopically implanted Lewis Lung Cell Carcinoma. (A) On Immunohistochemistry Lewis Lung Cancers showed only a weak positivity for the β3 integrin subunit, while αv staining was strong throughout the tumor. Positive staining for αv β3 was predominantly co-localized to the tumor cells, only partly to CD31 positive endothelial cells.(B) Tumor-bearing mice injected with the αvβ3 targeted NIRF probe IntegriSense680 showed a strong fluorescence signal from the tumor (left panel), while normal lung tissue did not render a detectable signal (center panel). NIRF signal was significantly decreased in mice pre-injected with a blocking agent as well as in chemotherapy treated mice (right panel, n = 3–5 for each scale bar).(C) Tumor-bearing lungs were excised and cells suspensions prepared after enzymatic digestion. Multicolor flow cytometry was performed after staining for CD31, CD51 (αv) and CD61 (β3) and propidium iodine (the latter not shown). Percentages in each quadrant of the dot plots give number of single positive, double positive and double negative cells (n = 3 replicates for each).

results confirmed the observation on IHC that especially tumor cells show a weak expression of the β3 subunit, while the αv subunit was expressed to a higher degree.

FMT-XCT Imaging of αvβ3 Expressing Lewis Lung Carcinomas

Hybrid FMT-XCT imaging could detect a positive fluorescence signal in Lewis Lung Carcinoma bearing mice injected with the αvβ3 targeted NIRF probe (Figure 3, *A–F*). Simultaneously acquired CT images could co-localize the fluorescence signal to the solid tumors. Fluorescent signal from lung tumors detected by FMT was confirmed by ex-vivo cryoslicing (Figure 3, *G-I*). To semi-quantify the fluorescence of orthotopic lung tumors we calculated a fluorescence ratio (Mean fluorescence in tumor/Mean fluorescence in reference lung tissue), which increased the signal from initial detectable tumor growth to one and two weeks after (1.6 ± 2.0 to 6.7 ± 7.0 to 11.3 ± 10.6, $P = .032$ one-way ANOVA, Figure *J*). Pre-injection of the mice with the RGD-based blocking peptide Cilengitide decreased the FMT fluorescence ratio of IntegriSense680 in tumor-bearing mice significantly (1.1 ± 0.7 versus 3.2 ± 1.7, $P = .015$ unpaired t test, Figure 4).

Therapy Response Assessment Using αvβ3 Targeted FMT-XCT

To detect early therapy response, Lewis Lung Carcinoma bearing mice were treated with an established NSCLC chemotherapy regimen of Cisplatin and Bevacizumab. Additionally we evaluated imaging of therapy response to the novel MEK inhibitor Refametinib (BAY 86–9766). Fluorescence imaging by hybrid FMT-XCT was performed in a similar manner as described in control mice (Figure 5*A-F*). While the NIRF signal for αvβ3 increased in non-treated mice over time, αvβ3 signal was stagnant at 1 and 2 weeks in chemotherapy treated mice (group difference $P = .002$, time difference $P = .0595$, interaction $P = .0123$, two-way ANOVA, Figure 5*G*). Both at 1 week and 2 week Bonferoni post-hoc test revealed a significant difference between control and treated mice. At the same time, non-treated tumors almost quadrupled in volume (30.9 to 47.9 to 118.6 mm^3), whereas treated tumors showed only a small, non-significant increase in volume (39.4 to 46.7 to 58.0 mm^3, group difference $P = .249$, time difference $P < .001$, interaction $P = .002$, 2-way ANOVA). Post hoc test revealed a significant differences between treated mice only at 2 weeks, but not at 1 week (Figure 5*H*). Refametinib caused similar effects compared to

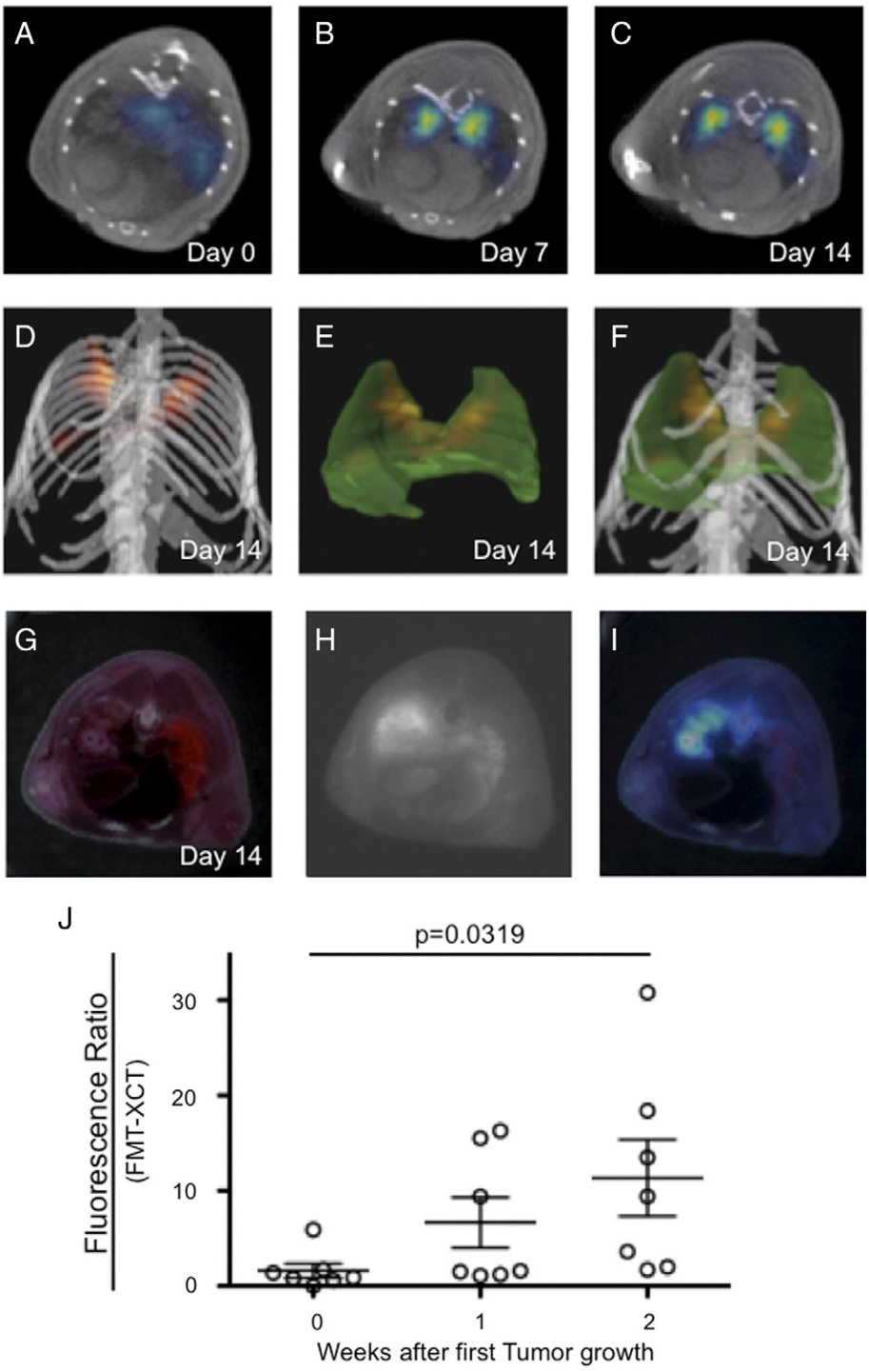

Figure 3. αvβ3-targeted FMT-XCT imaging of NCSLC bearing mice.FMT-XCT imaging revealed a positive NIRF signal originating from macroscopic tumor lesion bilaterally, which increased over time while the tumors progressed. A-C = transverse sections of hybrid FMT-XCT, D = volume rendering 3D image depicting tumor NIRF signal in yellow/red. E = 3D lung (green) together with tumor NIRF signal (yellow/red). F = volume rendering image of D and E combined. Fluorescence signal was confirmed by ex-vivo cryosclicing. G = color image, H = Fluorescence image, I = fused fluorescence-color image. Fluorescence ratio (Meant tumor signal/mean lung signal) increased during tumor progression (J).

Cisplatin/Bevacizumab. While the NIRF signal for αvβ3 increased in non-treated mice over time, αvβ3 signal was stagnant at one and two weeks in Refametinib treated mice (group difference $P = .0002$, time difference $P = .0543$, interaction $P = .0080$, two-way ANOVA, Figure 5*H*). Post-hoc test showed significant differences already at 1 week post treatment, but also at 2 weeks. Refametinib treated tumors showed stable volume (47.7 to 40.1 to 42.3.0 mm^3, group difference $P = .249$, time difference $P < .0001$, interaction $P = .002$, two-way ANOVA) compared to control mice, where only at 2 weeks the difference between treated and control mice was statistically significant in the post-hoc test. In summary, while tumor volume showed only differences at 2 weeks, FMT of αvβ3 expression

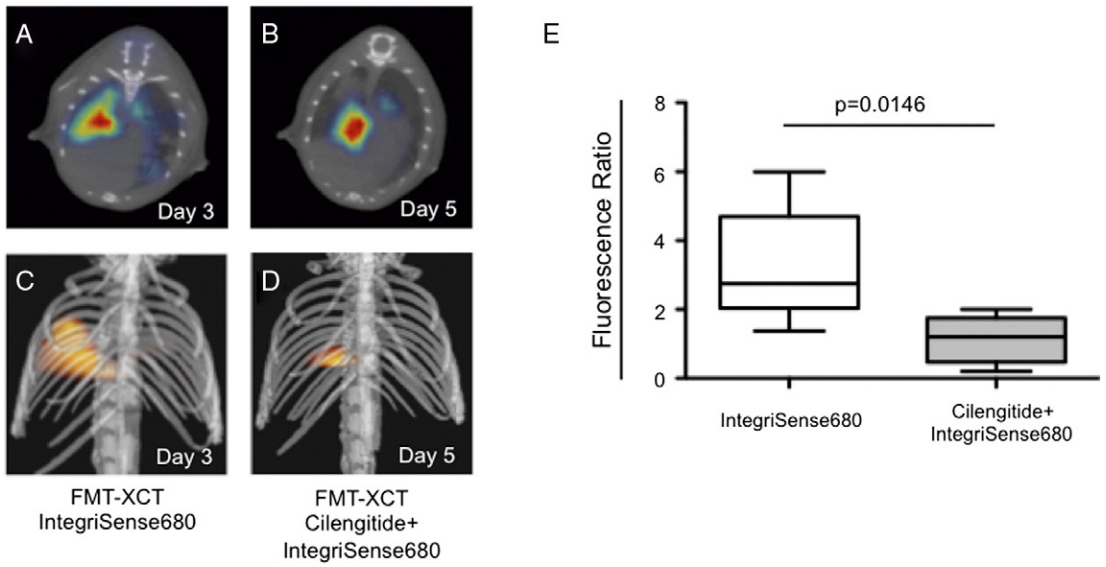

Figure 4. Competition/Blocking of the αvβ3 binding site by pre-injection of Cilengitide.Transversal (A and B) and 3D volume rendering (C and D) images demonstrate a significant decrease of the Fluorescence Ratio (E) for the αvβ3 targeted NIRF probe IntegriSense680 when the mice were injected with Cilengitide 15 minutes prior to application of the NIRF probe.

decreased significantly in treated compared to non-treated mice already at 1 week after start of treatment.

Discussion

Biomedical imaging has become a requisite tool in preclinical research, clinical trials and daily medical practice in oncology. While traditional imaging methodologies are restricted to morphologic observations and measurements, imaging in the era of molecular oncology is able to visualize the expression pattern and activity of particular cells, molecules and biological processes that are crucial to understand the in vivo behavior of tumors and their responsiveness or resistance to chemotherapeutic agents [10]. Lung cancer, still the leading cause of cancer mortality, is associated with a poor prognosis and even novel biological supplements targeting growth factors such as VEGF added to conventional chemotherapies only lead to a moderate increase in survival of a few months [8].

The poor prognosis of lung cancer is predominantly associated with its capacity to rapidly and efficiently invade adjacent tissue, blood and lymphatic vessels, causing subsequent metastasis. For the tumor cells to move and invade surrounding structures dynamic adhesion to extra cellular matrix components is essential. This decisive step of invasion and metastasis is mediated via a heterodimeric integrin receptor consisting of an α and β subunit. αvβ3 and α5β1 integrins, particularly important in lung cancer can be highly up regulated on the surface of tumor cells, activated or proliferating endothelial cells as well as activated macrophages [2]. Therefore those integrins have been proposed as an interesting target for molecular imaging. Molecular imaging of lung cancer is particularly important for early disease detection and monitoring of early therapy response. We have previously shown that using IntegriSense680, a αvβ3 targeted NIRF probe, allows early detection of NSCLC in a K-ras transgenic mouse model before macroscopic visible tumor lesions occur [15]. However, this approach was hampered by a strong background in non-tumorous lung tissue, as the developing lung in two week old 129/Sv-Kras^{tm3Tyj}/mice express those integrins to a high level, thereby significantly impairing a good target-to-background ratio [15]. To evaluate αvβ3 targeted fluorescence imaging for detection of early therapy response we therefore chose an orthotopic syngeneic model in adult Lewis Lung Carcinoma bearing mice. In our current study we show that: (1) Lewis Lung Carcinoma exhibit a sufficient expression of the αvβ3 integrin, which would potentially allow targeted imaging with a high sensitivity. (2) αvβ3 targeted fluorescence imaging using a hybrid FMT-XCT setup is feasible in a syngeneic orthotopic lung cancer model. (3) αvβ3 signal increases during tumor progression. (4) Integrin-targeted FMT-XCT imaging is able to depict tumor response to a standardized combination of Cisplatin/Bevacizumab as well as to a novel MEK inhibitor (Refametinib) already within 1 week whereas tumor size measured by CT at that time does not reveal any differences in treated versus untreated mice.

Lewis lung cell carcinoma is the most reproducible syngeneic mouse model for lung cancer so far and has been evaluated in depth for evaluating therapy response in vivo [19]. While the LLC tumor cells are frequently injected into the peritoneal cavity we chose to injected the tumor cells intravenously with subsequent orthotopic tumor growth in the lungs. This provides a couple of advantages, firstly the tumor microenvironment more accurately reflects the biology, and secondly we could take advantage of the FMT imaging approach, which is able to accurately depict and quantify fluorescence in deep tissue. While fluorescence from superficial tumors can be assessed reliably by planar fluorescence imaging, limited penetration depth, photon attenuation and scattering and weighting of signal towards surface activity, single projection viewing as well as non-linear effects of photon propagation lead to false interpretation of planar fluorescence data and require a tomographic fluorescence imaging approach [20]. Our in house built hybrid FMT-XCT device is able to simultaneously acquire fluorescence tomographic imaging data together with the corresponding μCT dataset. The CT data allows to correctly co-localize the fluorescence signal to the anatomical structures, but more importantly enables an accurate attenuation

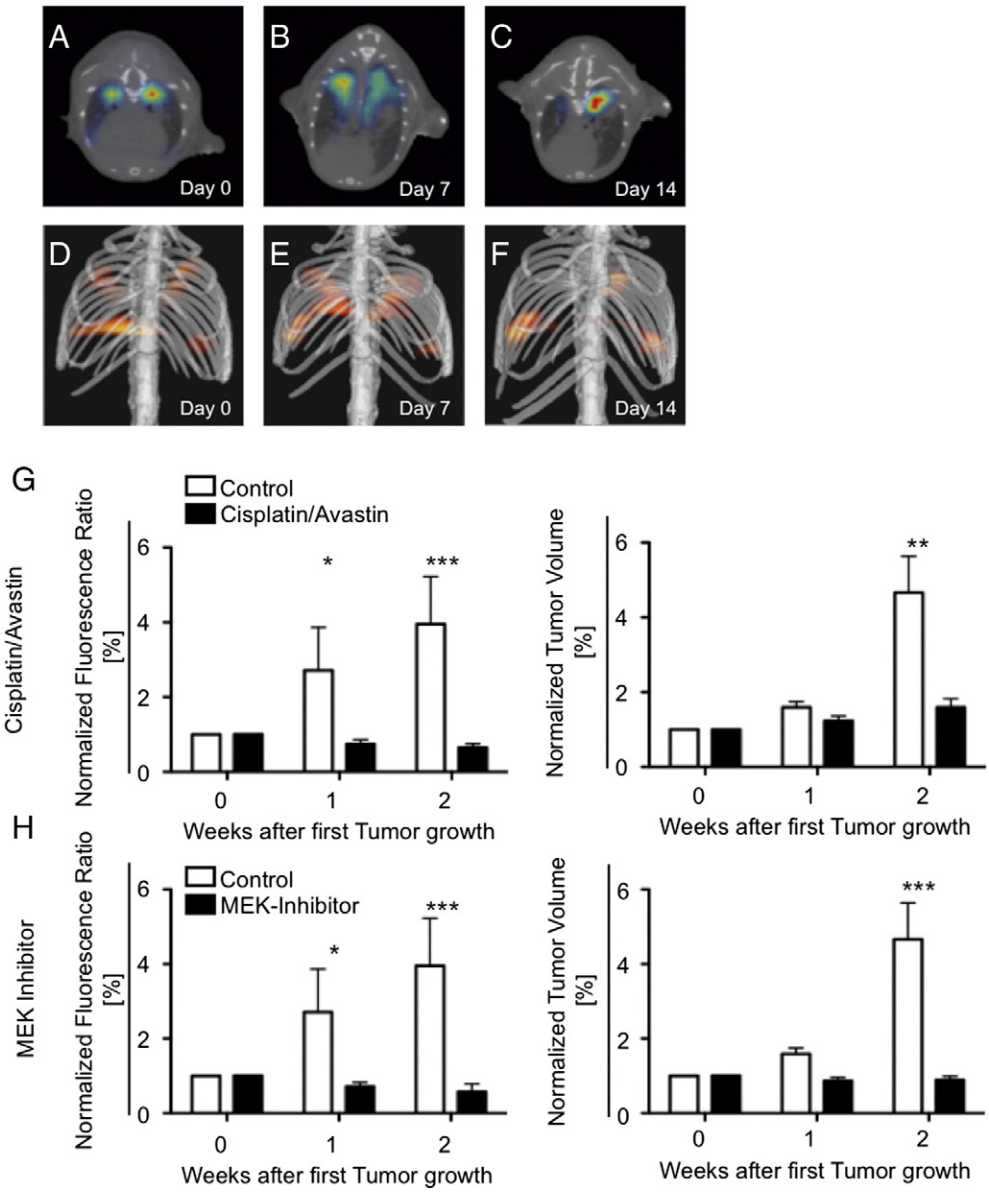

Figure 5. Assessment of therapy response by αvβ3 targeted FMT-XCT in Cisplatin/Bevacizumab treated mice.Fluorescence signal decreased in chemotherapy mice and was significantly lower compared to non-treated control mice already after one week of treatment whereas CT-based assessment of tumor volume was only significantly different from control mice at two weeks. A-C = transversal hybrid FMT-XCT scans, D-F = volume rendering 3D images, G = Bar graphs of normalized fluorescence ratio (fluorescence in each group at day 0 set to 1, left panel) and tumor volume (right panel) for Cisplatin/Bevacizumab treated versus control mice, H = Bar graphs of normalized fluorescence ratio (fluorescence in each group at day 0 set to 1, left panel) and tumor volume (right panel) for Refametinib treated versus control mice. Each bar consists of n = 3–6 mice, $*P < .05$, $**P < .01$, $***P < .001$.

correction, required for proper quantification of the molecular imaging signal [18,21].

Although αvβ3 poses a promising target for molecular imaging approaches, the variable degree of αvβ3 expression in various tumors has to be taken into account. Discrepancies in αvβ3 expression have been reported in lung adenocarcinomas [22]. A more recent study on human tissue samples revealed that human NSCLC are predominantly negative for αvβ3, while metastasis from this tumor exhibits increased levels of αvβ3 expression [23]. Therefore the distinct expression patterns of αvβ3 in various primary and secondary tumors has to be further elucidated and tumor heterogeneity is expected to be similarly reflected in specific integrin expression patterns. Additionally, it has to be stated that our imaging probe is not entirely specific for αvβ3, but also gets bound by αvβ5, which shares a similar chemical structure [15]. This, however, is not considered as a disadvantage, since both integrins exert at least similar functions and increased expression taking both molecules together will result in an increased signal-to-noise ratio and increased sensitivity. As αvβ5 has been reported to be highly expressed in primary NSCLC [2,23], it has to be taken into account that our imaging signature reported in this study does not derive solely from αvβ3, but potentially also from αvβ5 integrin. This might also explain, why, despite only a moderate

expression of the β3 subunit in our model (observed both by immunohistochemistry and flow cytometry), we still obtained a high fluorescence signal both ex-vivo and in-vivo from tumors injected with our NIRF probe.

We performed blocking studies using Cilengitide, a RGD mimetic compound, which has been evaluated as an anti-cancer-drug by itself [9,24,25]. Cilengitide led to effective blockade of IntegriSense680 binding leading to substantially decreased fluorescent signal. Thinking ahead, this mechanism could be incorporated in a theranostic approach, where fluorescently or radioactively labeled Cilengitide serves both as an imaging agent and anticancer drug.

Fluorescence imaging is always limited due to a limited penetration depth. Still, our approach carries substantial translational potential. Clinical applied fluorescence imaging has been shown to allow intraoperative tumor detection beyond the capacity of the surgeon's eye, allowing a significant increase in R0 resection [26]. In terms of non-invasive imaging, αvβ3 targeting can be similarly achieved by using non-fluorescence approaches using RGD based nuclear tracers [27,28], nanoparticles [13,14,29] and gadolinium chelates [30], which can be potentially translated into clinical practice. A preliminary study applying ^{18}F–galacto-RGD in 10 patients with NSCLC demonstrated the feasibility of performing such an approach in human lung cancer [31].

In summary, we show on the basis of a αvβ3 expressing orthotopic syngeneic NSCLC model, that integrin-targeted molecular imaging using a fluorescent reporter allows to track tumor progression and monitor early therapy response.

References

[1] Molina JR, Yang P, Cassivi SD, Schild SE, and Adjei AA (2008). Non-small cell lung cancer: epidemiology, risk factors, treatment, and survivorship. *Mayo Clin Proc* **83**, 584–594.

[2] Caccavari F, Valdembri D, Sandri C, Bussolino F, and Serini G (2010). Integrin signaling and lung cancer. *Cell Adh Migr* **4**, 124–129.

[3] Guo W and Giancotti FG (2004). Integrin signalling during tumour progression. *Nat Rev Mol Cell Biol* **5**, 816–826.

[4] Folkman J (2002). Role of angiogenesis in tumor growth and metastasis. *Semin Oncol* **29**, 15–18.

[5] Hynes RO (2002). A reevaluation of integrins as regulators of angiogenesis. *Nat Med* **8**, 918–921.

[6] Riabov V, Gudima A, Wang N, Mickley A, Orekhov A, and Kzhyshkowska J (2014). Role of tumor associated macrophages in tumor angiogenesis and lymphangiogenesis. *Front Physiol* **5**, 75.

[7] Desgrosellier JS and Cheresh DA (2010). Integrins in cancer: biological implications and therapeutic opportunities. *Nat Rev Cancer* **10**, 9–22.

[8] Johnson DH, Fehrenbacher L, Novotny WF, Herbst RS, Nemunaitis JJ, Jablons DM, Langer CJ, DeVore 3rd RF, Gaudreault J, and Damico LA, et al (2004). Randomized phase II trial comparing bevacizumab plus carboplatin and paclitaxel with carboplatin and paclitaxel alone in previously untreated locally advanced or metastatic non-small-cell lung cancer. *J Clin Oncol Off J Am Soc Clin Oncol* **22**, 2184–2191.

[9] Vansteenkiste J, Barlesi F, Waller CF, Bennouna J, Gridelli C, Goekkurt E, Verhoeven D, Szczesna A, Feurer M, and Milanowski J, et al (2015). Cilengitide combined with cetuximab and platinum-based chemotherapy as first-line treatment in advanced non-small-cell lung cancer (NSCLC) patients: results of an open-label, randomized, controlled phase II study (CERTO). *Ann Oncol* **26**, 1734–1740.

[10] Weissleder R and Pittet MJ (2008). Imaging in the era of molecular oncology. *Nature* **452**, 580–589.

[11] Decristoforo C, Hernandez Gonzalez I, Carlsen J, Rupprich M, Huisman M, Virgolini I, Wester HJ, and Haubner R (2008). 68Ga- and 111In-labelled DOTA-RGD peptides for imaging of alphavbeta3 integrin expression. *Eur J Nucl Med Mol Imaging* **35**, 1507–1515.

[12] Gaertner FC, Schwaiger M, and Beer AJ (2010). Molecular imaging of avb3 expression in cancer patients. *Q J Nucl Med Mol Imaging* **54**, 309–326.

[13] Boles KS, Schmieder AH, Koch AW, Carano RA, Wu Y, Caruthers SD, Tong RK, Stawicki S, Hu G, and Scott MJ, et al (2010). MR angiogenesis imaging with Robo4- vs. alphaVbeta3-targeted nanoparticles in a B16/F10 mouse melanoma model. *FASEB J* **24**, 4262–4270.

[14] Lee HY, Li Z, Chen K, Hsu AR, Xu C, Xie J, Sun S, and Chen X (2008). PET/MRI dual-modality tumor imaging using arginine-glycine-aspartic (RGD)-conjugated radiolabeled iron oxide nanoparticles. *J Nucl Med* **49**, 1371–1379.

[15] Ermolayev V, Mohajerani P, Ale A, Sarantopoulos A, Aichler M, Kayser G, Walch A, and Ntziachristos V (2015). Early recognition of lung cancer by integrin targeted imaging in K-ras mouse model. *Int J Cancer* **137**, 1107–1118.

[16] Haubner R, Weber WA, Beer AJ, Vabuliene E, Reim D, Sarbia M, Becker KF, Goebel M, Hein R, and Wester HJ, et al (2005). Noninvasive visualization of the activated alphavbeta3 integrin in cancer patients by positron emission tomography and [18F]Galacto-RGD. *PLoS Med* **2**, e70.

[17] Schulz RB, Ale A, Sarantopoulos A, Freyer M, Soehngen E, Zientkowska M, and Ntziachristos V (2010). Hybrid system for simultaneous fluorescence and x-ray computed tomography. *IEEE Trans Med Imaging* **29**, 465–473.

[18] Ale A, Siebenhaar F, Kosanke K, Aichler M, Radrich K, Heydrich S, Schiemann M, Bielicki I, Noel PB, and Braren R, et al (2013). Cardioprotective C-kit(+) bone marrow cells attenuate apoptosis after acute myocardial infarction in mice - in-vivo assessment with fluorescence molecular imaging. *Theranostics* **3**, 903–913.

[19] Kellar A, Egan C, and Morris D (2015). Preclinical Murine Models for Lung Cancer: Clinical Trial Applications. *Biomed Res Int* **2015**, 621324.

[20] Montet X, Figueiredo JL, Alencar H, Ntziachristos V, Mahmood U, and Weissleder R (2007). Tomographic fluorescence imaging of tumor vascular volume in mice. *Radiology* **242**, 751–758.

[21] Ale A, Ermolayev V, Herzog E, Cohrs C, de Angelis MH, and Ntziachristos V (2012). FMT-XCT: in vivo animal studies with hybrid fluorescence molecular tomography-X-ray computed tomography. *Nat Methods* **9**, 615–620.

[22] Friedlander M, Brooks PC, Shaffer RW, Kincaid CM, Varner JA, and Cheresh DA (1995). Definition of two angiogenic pathways by distinct alpha v integrins. *Science* **270**, 1500–1502.

[23] Vogetseder A, Thies S, Ingold B, Roth P, Weller M, Schraml P, Goodman SL, and Moch H (2013). alphav-Integrin isoform expression in primary human tumors and brain metastases. *Int J Cancer* **133**, 2362–2371.

[24] Albert JM, Cao C, Geng L, Leavitt L, Hallahan DE, and Lu B (2006). Integrin alpha v beta 3 antagonist Cilengitide enhances efficacy of radiotherapy in endothelial cell and non-small-cell lung cancer models. *Int J Radiat Oncol Biol Phys* **65**, 1536–1543.

[25] Mas-Moruno C, Rechenmacher F, and Kessler H (2010). Cilengitide: the first anti-angiogenic small molecule drug candidate design, synthesis and clinical evaluation. *Anticancer Agents Med Chem* **10**, 753–768.

[26] van Dam GM, Themelis G, Crane LM, Harlaar NJ, Pleijhuis RG, Kelder W, Sarantopoulos A, de Jong JS, Arts HJ, and van der Zee AG, et al (2011). Intraoperative tumor-specific fluorescence imaging in ovarian cancer by folate receptor-alpha targeting: first in-human results. *Nat Med* **17**, 1315–1319.

[27] Shi J, Jin Z, Liu X, Fan D, Sun Y, Zhao H, Zhu Z, Liu Z, Jia B, and Wang F (2014). PET imaging of neovascularization with (68)Ga-3PRGD2 for assessing tumor early response to Endostar antiangiogenic therapy. *Mol Pharm* **11**, 3915–3922.

[28] Trajkovic-Arsic M, Mohajerani P, Sarantopoulos A, Kalideris E, Steiger K, Esposito I, Ma X, Themelis G, Burton N, and Michalski CW, et al (2014). Multimodal molecular imaging of integrin alphavbeta3 for in vivo detection of pancreatic cancer. *Journal of nuclear medicine: official publication, Society of Nuclear Medicine* **55**, 446–451.

[29] Kazmierczak PM, Schneider M, Habereder T, Hirner-Eppeneder H, Eschbach RS, Moser M, Reiser MF, Lauber K, Nikolaou K, and Cyran CC (2016). alphavss3-Integrin-Targeted Magnetic Resonance Imaging for the Assessment of Early Antiangiogenic Therapy Effects in Orthotopic Breast Cancer Xenografts. *Invest Radiol* **51**, 746–755.

[30] Schmieder AH, Winter PM, Williams TA, Allen JS, Hu G, Zhang H, Caruthers SD, Wickline SA, and Lanza GM (2013). Molecular MR imaging of neovascular progression in the Vx2 tumor with alphavbeta3-targeted paramagnetic nanoparticles. *Radiology* **268**, 470–480.

[31] Beer AJ, Lorenzen S, Metz S, Herrmann K, Watzlowik P, Wester HJ, Peschel C, Lordick F, and Schwaiger M (2008). Comparison of integrin alphaVbeta3 expression and glucose metabolism in primary and metastatic lesions in cancer patients: a PET study using 18F-galacto-RGD and 18F-FDG. *J Nucl Med* **49**, 22–29.